MNRAS 000, 000–000 (0000) Preprint 15 December 2016 Compiled using MNRAS LATEX style file v3.0

SN 2015bp: adding to the growing population of transitional type Ia supernovae

Shubham Srivastav[1,2⋆], G. C. Anupama[1†], D. K. Sahu[1], C. D. Ravikumar[2]
[1] Indian Institute of Astrophysics, II Block Koramangala, Bangalore-560 034, India
[2] Department of Physics, University of Calicut, Malappuram-673635, India

arXiv:1612.04735v1 [astro-ph.SR] 14 Dec 2016

15 December 2016

ABSTRACT

Photometric and spectroscopic observations of type Ia supernova 2015bp are presented, spanning ∼ −6 to ∼ +141 days since B-band maximum. Also presented are unpublished HCT spectra of type Ia iPTF13ebh between −11 to +34 days since B-band maximum. SN 2015bp shows rapidly declining light curves with $\Delta m_{15}(B) = 1.72 \pm 0.04$. The I-band light curve shows a clear secondary maximum and peaks before the B-band maximum, placing SN 2015bp in the transitional category of SNe Ia. The spectral evolution of SN 2015bp resembles other transitional SNe Ia rather than 1991bg-like events. The C II λ6580 feature is detected in both SN 2015bp and iPTF13ebh, though it is present till the epoch of B-band maximum in the case of SN 2015bp. The velocity gradients of Si II λ6355 place SN 2015bp and iPTF13ebh in the FAINT subclass, whereas pseudo-equivalent widths of Si II features place them in the Cool (CL) subclass of SNe Ia. The bolometric light curve of SN 2015bp indicates that ∼ 0.2 $M_\odot$ of ^{56}Ni was synthesized in the explosion, with a total ejected mass of ∼ 0.9 $M_\odot$, suggesting a sub-Chandrasekhar mass white dwarf progenitor.

Key words: supernova: general – supernovae: individual: SN 2015bp – supernovae: individual: iPTF13ebh – galaxies: individual: NGC 5839

1 INTRODUCTION

Type Ia supernovae (SNe Ia) are characterized by the absence of hydrogen and helium features and presence of prominent absorption features of singly ionized silicon, magnesium, calcium and iron in spectra near maximum light (Filippenko 1997). Most SNe Ia follow the width-luminosity relation (Phillips 1993), making them powerful standardizable cosmological distance indicators. This property of SNe Ia was instrumental in the discovery of accelerated expansion of the universe and dark energy (Riess et al. 1998; Perlmutter et al. 1999). The progenitors of SNe Ia are widely believed to be accreting carbon-oxygen white dwarfs (WDs) in close binary systems (Hoyle & Fowler 1960). The explosion is thus caused by thermonuclear runaway in the degenerate WD (Nomoto et al. 1984). However, the nature of the companion and details of the explosion physics are still not clearly understood (Hillebrandt & Niemeyer 2000; Howell 2011; Hillebrandt et al. 2013). Different progenitor scenarios and explosion mechanisms have been proposed to explain the observed diversity in SNe Ia (see Maoz et al. 2014). Explosion of a Chandrasekhar mass WD via a delayed detonation (Khokhlov 1991), also called deflagration to detonation transition (DDT), is a popular mechanism which could possibly account for most SNe Ia (Mazzali et al. 2007). However, Scalzo et al. (2014b) suggested that a sizeable fraction (25-50 %) of SNe Ia are sub-Chandrasekhar mass explosions. In the sub-Chandrasekhar mass regime, double detonation (eg. Woosley & Weaver 1994; Livne & Arnett 1995) is the most well studied explosion mechanism.

Although a majority (∼ 70%) of SNe Ia fall within the 'normal' category, ∼ 18% are subluminous 1991bg-like events, the remaining being overluminous SN 1991T-like and peculiar SN 2002cx-like events (Li et al. 2011). Previous studies have noted the conspicuous dearth of 'transitional' Ia events with $1.5 \lesssim \Delta m_{15}(B) \lesssim 1.7$ (eg. Prieto et al. 2006; Ashall et al. 2016b). The question remains whether this is due to a selection effect, or that transitional SNe Ia are intrinsically rare events at the junction of a bimodal distribution (Ashall et al. 2016b). Krisciunas et al. (2009) noticed a bimodality in the NIR luminosity of SNe Ia, wherein events whose NIR light curves peak before the B-band light curve were seen to show a normal luminosity (regardless of $\Delta m_{15}(B)$), whereas those events with later NIR maxima were seen to be subluminous in all bands. Recently, Hsiao et al. (2015, hereafter H15) defined transitional SNe Ia as the class of fast declining events whose NIR maxima pre-

⋆ E-mail : ssrivastav@iiap.res.in
† E-mail : gca@iiap.res.in

© 0000 The Authors

cede the B-band maximum, as opposed to the subluminous SN 1991bg class of events which show late NIR maxima. This is owing to events like SN 1986G (Phillips et al. 1987) and SN 2003gs (Krisciunas et al. 2009), which show Ti II features in their early spectra, but they also show early NIR maxima and their overall properties and luminosity is intermediate to normal-bright and 1991bg-like events. Examples of well studied transitional events in the literature include SN 1986G (Phillips et al. 1987), SN 2003hv (Leloudas et al. 2009), SN 2003gs (Krisciunas et al. 2009), SN 2004eo (Pastorello et al. 2007), SN 2007on (Stritzinger et al. 2011), SN 2009an (Sahu et al. 2013), SN 2011iv (Foley et al. 2012), SN 2012ht (Yamanaka et al. 2014) and iPTF13ebh (H15). With intermediate photometric and spectroscopic properties, transitional SNe Ia signify a link between normal-bright and subluminous 1991bg-like events, suggesting a continuous range of properties and possibly a common explosion mechanism (H15; Ashall et al. 2016b).

In this paper, we present the results of photometric and spectroscopic observations of transitional type Ia supernova SN 2015bp. SN 2015bp was discovered on 2015 March 16.49 UT by the Catalina Real-Time Transient Survey (CRTS) as SNhunt281 and independently by Stan Howerton (CBAT TOCP). SN 2015bp was found at the position RA = $15^h\,05^m\,30^s.1$, Dec. = $+01^\circ\,38'\,02''.4$, at a discovery magnitude of 19.2 in V band. The transient was offset by ~ 39 arcsec from the S0 galaxy NGC 5839, which has a redshift of z = 0.004 (NED). It was subsequently classified as a 1991bg-like event by Jha et al. (2015) using a spectrum obtained on March 18.0 UT with the DEIMOS spectrograph on Keck II. We also present unpublished spectra of transitional Ia iPTF13ebh, which showed a fast decline with $\Delta m_{15}(B) = 1.79$ and displayed strong carbon features in its NIR spectra (H15).

2 DATA REDUCTION

2.1 Optical Photometry

Photometric monitoring of SN 2015bp began on 2015 March 25 using the Himalayan Faint Object Spectrograph Camera (HFOSC) instrument mounted on the 2-m Himalayan Chandra Telescope at the Indian Astronomical Observatory (IAO) in Hanle, India. The HFOSC is equipped with a 2K × 4K SITe CCD, of which the central 2K × 2K region was used for imaging observations. The pixels are 15µm × 15µm each in size. The field of view in imaging mode is 10 arcmin × 10 arcmin, with an image scale of 0.3 arcsec pixel^{-1}. Optical photometry was obtained on 23 epochs spanning −5.9 to +140.8 d since B-band maximum, using the Bessell $UBVRI$ filters available with the HFOSC. Landolt standard fields (Landolt 1992) were observed under photometric conditions on three nights in order to calibrate the supernova field. Standard fields PG0918+029 and PG1323-086 were observed on the night of 2015 April 04, PG2213-006 and PG0231+051 on the night of 2015 August 19, and PG0918+029, PG0942-029 and PG1323-006 were observed on the night of 2016 April 12.

Data reduction was carried out in the standard way using various packages available in the Image Reduction and Analysis Facility (IRAF[1]). Aperture photometry was performed on the standard stars. In order to correct for atmospheric extinction, average extinction coefficients for the site (Stalin et al. 2008) were used. Average colour terms for the HFOSC system were used to compute the photometric zero-points during the calibration nights. Several local standards in the supernova field were calibrated using the estimated zero-points on the calibration nights. The local standards are identified in Figure 1. The $UBVRI$ magnitudes of the local standards, averaged over three nights, are listed in Table 1. Photometry was performed on the supernova and local standards using the profile-fitting method and the SN magnitudes were derived differentially using the calibrated magnitudes of the local standards. Nightly photometric zero-points were computed using the local standards and applied to the supernova instrumental magnitudes. Colour corrections calculated using the local standards were incorporated in the zero-point calculations. The summary of photometric observations and magnitudes of SN 2015bp are given in Table 2.

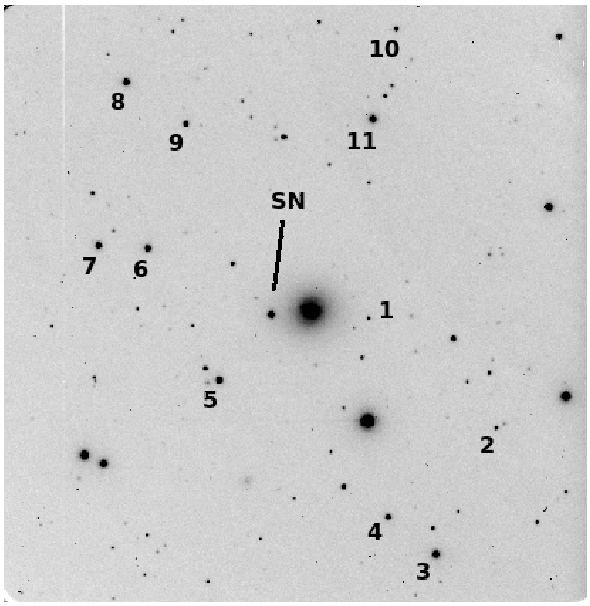

Figure 1. Identification chart for SN 2015bp. North is up and East is to the left. The field of view is 10′ × 10′. The local standards used for calibration are also indicated.

2.2 *Swift* UVOT Photometry

SN 2015bp was followed up by the UVOT instrument (Roming et al. 2005) on the *Swift* satellite (Gehrels et al. 2004) from 2015 March 19 (−11.9 d) to 2015 May 15 (+44.4 d), where the phase denotes time since B-band maximum. The images were obtained in three broadband optical filters v (5468 Å), b (4392 Å), u (3465 Å) and three broadband UV filters $uvw1$ (2600 Å), $uvm2$ (2246 Å), $uvw2$ (1928 Å). The UVOT data for SN 2015bp were downloaded from

[1] IRAF is distributed by the National Optical Astronomy Observatories, which are operated by the Association of Universities for Research in Astronomy, Inc., under cooperative agreement with the National Science Foundation.

Table 1. $UBVRI$ Magnitudes of local standards in the field of SN 2015bp.

ID	U	B	V	R	I
1	16.963 ± 0.012	17.084 ± 0.035	16.860 ± 0.006	16.738 ± 0.022	16.564 ± 0.001
2	17.276 ± 0.028	17.397 ± 0.026	16.733 ± 0.010	16.350 ± 0.024	15.999 ± 0.014
3	14.337 ± 0.036	14.659 ± 0.024	14.148 ± 0.002	13.803 ± 0.013	13.471 ± 0.006
4	16.112 ± 0.022	15.925 ± 0.016	15.196 ± 0.019	14.783 ± 0.019	14.413 ± 0.022
5	15.176 ± 0.009	15.159 ± 0.019	14.484 ± 0.029	14.096 ± 0.023	13.722 ± 0.007
6	15.461 ± 0.006	15.270 ± 0.022	14.537 ± 0.012	14.142 ± 0.004	13.800 ± 0.003
7	15.506 ± 0.007	15.356 ± 0.022	14.648 ± 0.035	14.237 ± 0.029	13.851 ± 0.011
8	16.212 ± 0.024	15.656 ± 0.003	14.734 ± 0.012	14.193 ± 0.008	13.752 ± 0.021
9	17.880 ± 0.031	16.836 ± 0.015	15.752 ± 0.016	15.150 ± 0.016	14.655 ± 0.020
10	17.210 ± 0.043	17.044 ± 0.018	16.280 ± 0.014	15.860 ± 0.001	15.448 ± 0.006
11	15.735 ± 0.034	15.227 ± 0.007	14.291 ± 0.012	13.782 ± 0.007	13.313 ± 0.005

Table 2. Optical $UBVRI$ photometry of SN 2015bp.

Date (yyyy/mm/dd)	JD (245 7000+)	Phase* (days)	U	B	V	R	I
2015/03/25	107.48	−5.85	13.82 ± 0.04	14.32 ± 0.02	14.24 ± 0.02	14.06 ± 0.02	14.06 ± 0.02
2015/03/27	109.23	−4.10	13.69 ± 0.03	14.12 ± 0.02	14.02 ± 0.02	13.85 ± 0.01	13.90 ± 0.02
2015/03/31	113.26	−0.07	13.63 ± 0.05	13.98 ± 0.03	13.81 ± 0.03	13.75 ± 0.02	13.93 ± 0.03
2015/04/01	114.35	+1.02			13.82 ± 0.02	13.74 ± 0.02	13.94 ± 0.01
2015/04/02	115.22	+1.89	13.86 ± 0.06	14.03 ± 0.04	13.82 ± 0.02	13.75 ± 0.02	13.94 ± 0.03
2015/04/05	118.28	+4.95			13.88 ± 0.03	13.90 ± 0.04	14.13 ± 0.02
2015/04/08	121.32	+7.99	14.49 ± 0.02	14.62 ± 0.02	14.11 ± 0.03	14.16 ± 0.02	14.31 ± 0.02
2015/04/09	122.31	+8.98	14.72 ± 0.04	14.79 ± 0.01	14.19 ± 0.03	14.22 ± 0.02	14.33 ± 0.01
2015/04/10	123.22	+9.89	14.86 ± 0.02	14.92 ± 0.02	14.26 ± 0.02	14.26 ± 0.02	14.32 ± 0.01
2015/04/11	124.34	+11.01	15.07 ± 0.02	15.10 ± 0.02	14.35 ± 0.02	14.30 ± 0.02	14.32 ± 0.02
2015/04/13	126.32	+12.99	15.39 ± 0.02	15.36 ± 0.02	14.45 ± 0.02	14.30 ± 0.02	14.24 ± 0.02
2015/04/15	128.21	+14.88	15.73 ± 0.02	15.68 ± 0.01	14.61 ± 0.01	14.36 ± 0.02	14.22 ± 0.02
2015/04/17	130.48	+17.15			14.74 ± 0.04	14.46 ± 0.02	14.22 ± 0.03
2015/04/18	131.37	+18.04		16.09 ± 0.02	14.85 ± 0.02	14.52 ± 0.02	14.24 ± 0.03
2015/04/24	137.33	+24.00	16.57 ± 0.03	16.57 ± 0.01	15.38 ± 0.02	15.03 ± 0.02	14.62 ± 0.02
2015/04/28	141.40	+28.07	16.73 ± 0.02	16.80 ± 0.01	15.65 ± 0.01	15.33 ± 0.02	14.97 ± 0.02
2015/04/29	142.20	+28.87	16.79 ± 0.03	16.85 ± 0.02	15.66 ± 0.02	15.38 ± 0.02	15.03 ± 0.02
2015/05/01	144.29	+30.96	16.87 ± 0.02	16.91 ± 0.02	15.83 ± 0.03	15.58 ± 0.05	15.15 ± 0.04
2015/05/05	148.26	+34.93	17.01 ± 0.03	17.03 ± 0.02	15.94 ± 0.03	15.64 ± 0.02	15.34 ± 0.03
2015/05/17	160.23	+46.90		17.33 ± 0.02	16.35 ± 0.01	16.16 ± 0.01	16.01 ± 0.02
2015/05/22	165.39	+52.06		17.42 ± 0.01	16.51 ± 0.02	16.35 ± 0.02	16.25 ± 0.01
2015/07/24	228.13	+114.80			18.26 ± 0.03	18.34 ± 0.04	18.27 ± 0.03
2015/08/19	254.15	+140.82	19.95 ± 0.05	19.04 ± 0.05	18.70 ± 0.08	18.77 ± 0.10	18.67 ± 0.09

*time since B-band max (JD 2457113.33)

the *Swift* archive. Data reduction was performed using HEASOFT (High Energy Astrophysics SOFTware) following the prescriptions of Poole et al. (2008) and Brown et al. (2009). The *uvotsource* task was used to extract the supernova magnitudes. Updated zero-points and effective area curves for the *Swift* UVOT filters provided by Breeveld et al. (2011) were used for the photometry. An aperture of 5 arcsec was used for the supernova for most images except for the last few epochs, when a smaller aperture of 3.5 arcsec was chosen for better S/N since the supernova had become quite faint. An aperture correction prescribed by Poole et al. (2008) was applied whenever the smaller aperture was used. Sky regions of 5 arcsec each were chosen in the supernova vicinity for estimation of the background. The estimated *Swift* UVOT Vega magnitudes are listed in Table 3. The UV magnitudes of iPTF13ebh were obtained from the Swift Optical/Ultraviolet Supernova Archive (SOUSA; Brown et al. 2014).

2.3 Optical Spectroscopy

Optical spectra of SN 2015bp were obtained on 13 epochs between −4.1d to +93.9d since B-band maximum, while spectra of iPTF13ebh were obtained on 11 epochs spanning −11.1d and +33.7d since B-band maximum. The observations were made using Grisms Gr7 (3500-7800 Å) and Gr8 (5200-9250 Å) at a spectral resolution of ∼ 7 Å. Arc lamp spectra of FeAr and FeNe were used for wavelength calibration. Spectrophotometric standard stars HZ 44, Feige 34 and Feige 110 (Oke 1990) were used for flux calibration. On those nights where standard spectra were not obtained, the response curves obtained during nearby nights were used. The flux calibrated spectra in Gr7 and Gr8 were combined

Table 3. *Swift* UVOT photometry of SN 2015bp.

Date	JD (245 7000+)	Phase* (days)	uvw2	uvm2	uvw1	u	b	v
2015/03/19	101.43	−11.90	19.16 ± 0.19	17.49 ± 0.12	18.01 ± 0.11	16.15 ± 0.06	16.25 ± 0.05	15.99 ± 0.07
2015/03/25	107.09	−6.24	16.51 ± 0.05	15.16 ± 0.05	16.72 ± 0.08	13.82 ± 0.04	14.37 ± 0.04	14.38 ± 0.03
2015/03/27	109.32	−4.01	16.18 ± 0.08	14.90 ± 0.06	16.52 ± 0.09	13.65 ± 0.04	14.11 ± 0.04	14.02 ± 0.05
2015/03/30	111.67	−1.66	16.23 ± 0.08	15.01 ± 0.06	16.59 ± 0.09	13.63 ± 0.04	13.89 ± 0.04	13.81 ± 0.05
2015/03/31	112.95	−0.38	16.39 ± 0.07	15.20 ± 0.05	16.77 ± 0.08	13.75 ± 0.04	13.88 ± 0.04	13.78 ± 0.04
2015/04/02	115.41	+2.08	16.68 ± 0.08	15.51 ± 0.06	16.94 ± 0.09	14.05 ± 0.04	13.95 ± 0.04	13.82 ± 0.04
2015/04/09	122.00	+8.67	17.68 ± 0.12	16.20 ± 0.08	17.77 ± 0.12	15.02 ± 0.05	14.54 ± 0.04	14.07 ± 0.05
2015/04/12	124.91	+11.58	17.80 ± 0.15	16.66 ± 0.11	18.39 ± 0.20	15.47 ± 0.07	15.06 ± 0.05	14.27 ± 0.06
2015/04/21	134.35	+21.02	18.43 ± 0.19	17.43 ± 0.15	18.30 ± 0.19	16.56 ± 0.11	16.18 ± 0.07	15.04 ± 0.07
2015/04/27	139.90	+26.57	18.94 ± 0.24	17.73 ± 0.16	18.56 ± 0.19	16.75 ± 0.12	16.66 ± 0.08	15.42 ± 0.08
2015/05/02	145.11	+31.78	19.02 ± 0.18	17.82 ± 0.13	18.83 ± 0.17	17.14 ± 0.11	16.81 ± 0.07	15.79 ± 0.07
2015/05/07	150.14	+36.81		18.00 ± 0.11		17.26 ± 0.10	16.88 ± 0.07	
2015/05/10	153.30	+39.97	>18.70	18.12 ± 0.25	18.73 ± 0.23	17.48 ± 0.21	17.14 ± 0.13	16.07 ± 0.13
2015/05/15	157.69	+44.36	19.04 ± 0.25	18.38 ± 0.22	>19.15	17.57 ± 0.18	16.84 ± 0.08	16.35 ± 0.13

*time since B-band max (JD 2457113.33)

with an appropriate scale factor to obtain a single spectrum. The final spectra were scaled to an absolute flux level using the broadband $UBVRI$ magnitudes. For iPTF13ebh, the broadband magnitudes provided by H15 were used to scale the spectra. Telluric lines have not been removed from the spectra. The journal of spectroscopic observations for SN 2015bp and iPTF13ebh is shown in Tables 4 and 5, respectively.

3 PHOTOMETRIC ANALYSIS

3.1 Light Curves

SN 2015bp reached B-band maximum on 2015 March 31 (JD 2457113.33). The HCT optical $UBVRI$ and *Swift* UVOT UV light curves of SN 2015bp are shown in Figure 2. The light curves show a fast decline with $\Delta m_{15}(B) = 1.72 \pm 0.04$. However, the secondary maximum in I-band and shoulder in R-band places SN 2015bp closer to normal SNe Ia rather than 1991bg-like events. In Figure 3, we compare the $BVRI$ light curves of SN 2015bp with a few other well studied transitional SNe Ia which include iPTF13ebh (H15), SN 2009an (Sahu et al. 2013), SN 2007on (Stritzinger et al. 2011), SN 2004eo (Pastorello et al. 2007) and SN 2003hv (Leloudas et al. 2009). For iPTF13ebh and SN 2007on, the published magnitudes were in B, V and SDSS $ugri$ filters. In order to facilitate light curve comparison, the SDSS magnitudes were converted to R, I magnitudes using the transformation equations provided by Lupton (2005). The light curves of the comparison SNe were normalized with respect to their peak magnitudes, and shifted in time to match the epoch of their respective B-band maxima with that of SN 2015bp. The $BVRI$ light curves of SN 2015bp and iPTF13ebh are quite similar, albeit iPTF13ebh shows a slightly faster decline ($\Delta m_{15}(B) = 1.79$).

The decline rate parameter $\Delta m_{15}(B)$ is sensitive to the amount of reddening suffered by the supernova (Phillips et al. 1999). For faster declining events, the $\Delta m_{15}(B)$ ceases to remain a good discriminator between slower and faster evolving events and a reliable indicator of intrinsic colors and light curve shapes (Burns et al. 2014). This is because faster declining SNe Ia enter the linear decline phase at earlier times (Folatelli et al. 2010; Burns et al. 2011).

The timing of the maxima in the NIR light curves relative to B-band is useful in distinguishing transitional SNe Ia and 1991bg-like SNe Ia (Krisciunas et al. 2009). SNe Ia which peak at later epochs in NIR bands have been found to belong exclusively in the fast declining category ($\Delta m_{15}(B) > 1.7$) and are subluminous in all bands (Krisciunas et al. 2009; Phillips 2012; Burns et al. 2014). Like in normal SNe Ia, the I-band maxima for SN 2015bp and iPTF13ebh (H15) occur a few days before their B-band maxima.

The secondary peak in NIR light curves, occurring 20-30 days after the primary peak, is a ubiquitous feature in SNe Ia. The secondary peak is a consequence of a change in opacity when the ionization state in the ejecta changes due to recombination in iron group elements (Kasen 2006). The strength of the I-band secondary peak was shown to be correlated with $\Delta m_{15}(B)$ by Hamuy et al. (1996), who found that faster declining events show weaker secondary maxima. The I-band secondary maximum is either in the form of a weak plateau or entirely missing in subluminous SNe Ia like SN 1991bg (Leibundgut et al. 1993), SN 1998de (Modjaz et al. 2001), SN 1999by (Garnavich et al. 2004), SN 2005bl (Taubenberger et al. 2008) and other 1991bg-like events. In order to quantify the strength of the I-band secondary maximum relative to the primary, Krisciunas et al. (2001) introduced a new empirical parameter $\langle f_\lambda(i) \rangle_{20-40}$, defined as the average flux in the I-band between 20 to 40 days since B maximum (normalized to the peak I-band flux). Burns et al. (2014, Figure 6) found a correlation between $\langle f_\lambda(i) \rangle_{20-40}$ and $\Delta m_{15}(B)$, reaffirming the results of Hamuy et al. (1996). However, the fast declining events ($\Delta m_{15}(B) \gtrsim 1.7$) were seen to separate into two clusters - one with stronger and the other with weaker secondary I-band maxima, respectively (Burns et al. 2014). Evidently, the cluster with weaker I-band maxima represents the 1991bg-like subclass of events, whereas the cluster with stronger I-band maxima is populated by transitional

Date (yyyy/mm/dd)	JD 245 7000+	Phase* (days)	Range (Å)
2015/03/27	109.25	−4.08	3500-7800; 5200-9250
2015/03/31	113.29	−0.04	3500-7800; 5200-9250
2015/04/02	115.24	+1.91	3500-7800; 5200-9250
2015/04/03	116.22	+2.89	3500-7800; 5200-9250
2015/04/05	118.25	+4.92	3500-7800; 5200-9250
2015/04/08	121.33	+8.00	3500-7800; 5200-9250
2015/04/09	122.33	+9.00	3500-7800; 5200-9250
2015/04/10	123.24	+9.91	3500-7800; 5200-9250
2015/04/15	128.24	+14.91	3500-7800; 5200-9250
2015/04/29	142.23	+28.90	3500-7800; 5200-9250
2015/05/03	146.25	+32.92	3500-7800; 5200-9250
2015/05/22	165.40	+52.07	3500-7800; 5200-9250
2015/07/03	207.23	+93.90	3500-7800; 5200-9250

*time since B-band max (JD 2457113.33)

Table 4. Log of spectroscopic observations of SN 2015bp.

Date (yyyy/mm/dd)	JD 245 6000+	Phase* (days)	Range (Å)
2013/11/15	612.29	−11.13	3500-7800; 5200-9250
2013/11/16	613.37	−10.05	3500-7800; 5200-9250
2013/11/17	614.31	−9.11	3500-7800; 5200-9250
2013/11/19	616.29	−7.13	3500-7800; 5200-9250
2013/11/20	617.34	−6.08	3500-7800; 5200-9250
2013/11/24	621.35	−2.07	3500-7800; 5200-9250
2013/11/28	625.37	+1.95	3500-7800; 5200-9250
2013/12/04	631.37	+7.95	3500-7800
2013/12/18	645.32	+21.9	3500-7800; 5200-9250
2013/12/28	655.26	+31.84	3500-7800; 5200-9250
2013/12/30	657.15	+33.73	3500-7800; 5200-9250

*time since B-band max (JD 2456623.42)

Table 5. Log of spectroscopic observations of iPTF13ebh.

events whose overall photometric and spectroscopic properties are not so extreme. With $\langle f_\lambda(i)\rangle_{20-40} = 0.37$ and 0.34, respectively, both SN 2015bp and iPTF13ebh fit in with the transitional cluster showing stronger I-band secondary maxima.

3.2 Color Curves

The color curves of SNe Ia evolve towards red after maximum light due to recombination of Fe III to Fe II in the SN ejecta, which causes line blanketing in the B-band while increasing emissivity at longer wavelengths (Kasen & Woosley 2007). In faster declining events with cooler ejecta, the recombination occurs at earlier epochs, resulting in a rapid color evolution. The color evolution of SN 2015bp is shown in Figure 4, along with those of iPTF13ebh, SN 2009an, SN 2007on, SN 2004eo and SN 2003hv. The color curves were corrected for a Galactic reddening of $E(B-V)_{MW} = 0.046$ for SN 2015bp, $E(B-V)_{MW} = 0.068$ for iPTF13ebh, $E(B-V)_{MW} = 0.019$ for SN 2009an, $E(B-V)_{MW} = 0.01$ for SN 2007on, $E(B-V)_{MW} = 0.109$ for SN 2004eo and $E(B-V)_{MW} = 0.016$ for SN 2003hv. In addition, a host extinction component of $E(B-V)_{host} = 0.05$ for iPTF13ebh (H15) and $E(B-V)_{host} = 0.089$ for SN 2009an (Sahu et al. 2013) was also taken into account. The reddening correction was done using a standard reddening law (Cardelli et al. 1989) for $R_V = 3.1$. The Galactic reddening values are taken from Schlafly & Finkbeiner (2011), who derived it from the dust maps of Schlegel et al. (1998).

At its reddest, the $(B-V)$ color curve of SN 2015bp attains a value of 1.21 ± 0.03, occurring ~ 17 days after B-band maximum. Burns et al. (2014) found a strong correlation between the time of $(B-V)$ maximum and $\Delta m_{15}(B)$ and defined a new color stretch parameter, $s_{BV} = t_{max}/30$ days, where t_{max} is the time of maximum for the $(B-V)$ color curve. However, the correlation was seen to break down for fast decliners with $\Delta m_{15}(B) \gtrsim 1.7$ (Burns et al. 2014). With $\Delta m_{15}(B) = 1.72$, SN 2015bp is at the border of normal SNe Ia which follow the correlation between s_{BV} and Δm_{15}, and the fast decliners which do not. The $(B-V)$ color curves of SN 2015bp ($s_{BV} = 0.57$) and iPTF13ebh ($s_{BV} = 0.63$, H15) are similar, both objects reaching $(B-V)_{max} \sim 1.2$. SN 2007on ($s_{BV} = 0.55$) and SN 2003hv ($s_{BV} = 0.76$) attain smaller values of $(B-V)_{max} \sim 1.05$, SN 2007on evolving slightly faster and SN 2003hv slower relative to SN 2015bp.

According to the relation provided by Burns et al. (2014, Equation 3), the $(B-V)$ color curves of normal SNe Ia with $\Delta m_{15}(B) \sim 1.1$ peak ~ 30 days after B max-

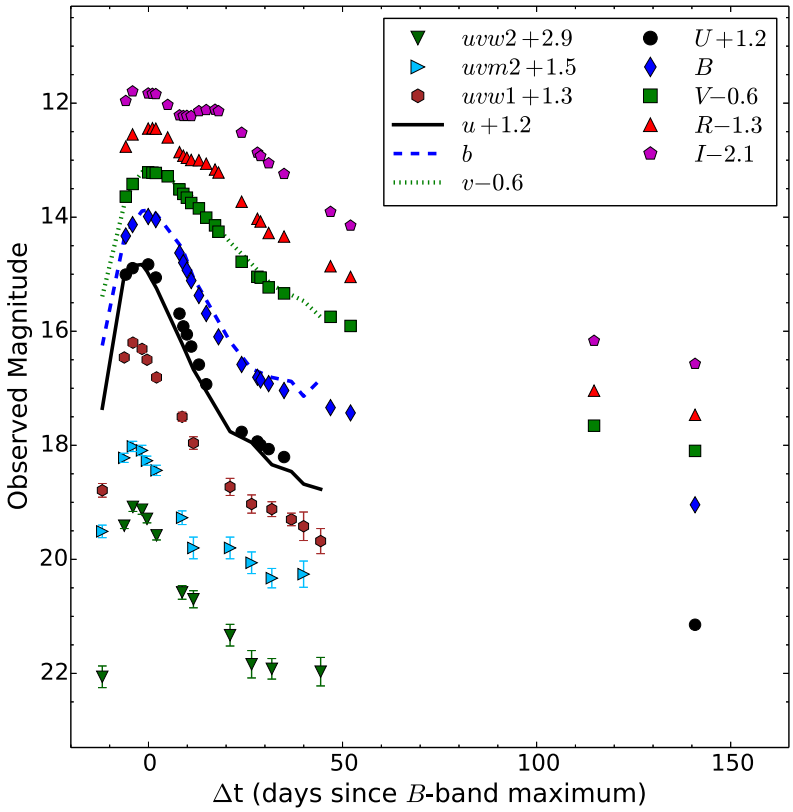

Figure 2. HCT Optical $UBVRI$ and *Swift* UV light curves of SN 2015bp. The light curves are shifted along y-axis for clarity. The typical errors on $UBVRI$ magnitudes are within the symbol sizes.

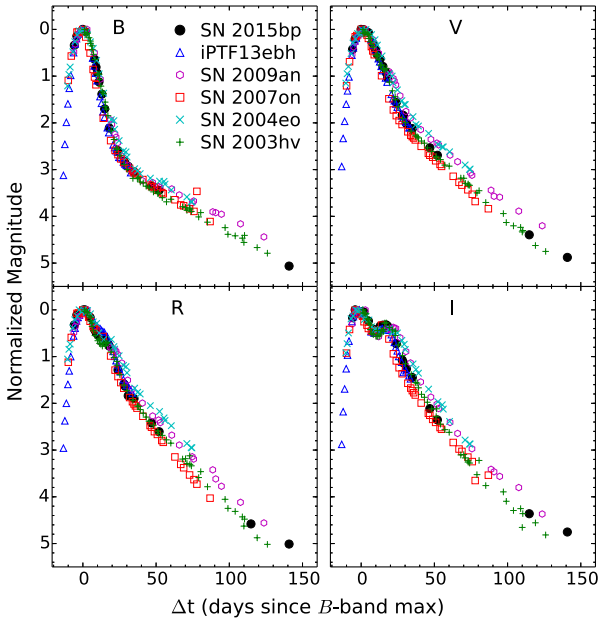

Figure 3. Light curve comparison of SN 2015bp with iPTF13ebh (H15), SN 2009an (Sahu et al. 2013), SN 2007on (Stritzinger et al. 2011), SN 2004eo (Pastorello et al. 2007) and SN 2003hv (Leloudas et al. 2009). The light curves of the comparison SNe have been shifted as described in the text.

imum. However, the $(B-V)$ color curves of SN 2015bp and iPTF13ebh peak within 20 days of B maximum. The rapid but otherwise normal color evolution of SN 2015bp and iPTF13ebh is consistent with their narrow, fast declining light curves.

The UV-optical colors of normal SNe Ia are known to be remarkably homogeneous (Milne et al. 2010). The $(uvw1-V)$ color curve attains a blue minimum ~ 5 days before B maximum, followed by a reddening till ~ 20 days (Milne et al. 2010). Further, Milne et al. (2013) suggested a bimodal distribution based on the $(uvw1-V)$ color curve into two main groups - NUV-blue and NUV-red. SN 2015bp attains a blue minimum of $(uvw1-V)_{min} \approx 0.75$, placing it in the NUV-blue category. Unlike SN 2015bp, iPTF13ebh is placed in the NUV-red category (H15). In Figure 5, we show the $(uvw1-V)$ color evolution of SN 2015bp and iPTF13ebh.

3.3 Host Reddening for SN 2015bp

There are several methods available for estimating the line of sight reddening suffered by SNe Ia in their host environment. The slope of the $(B-V)$ color curve between 30 to 90 days since maximum light is remarkably homogeneous for SNe Ia which have suffered little or no reddening (Lira 1995). The slope of the observed $(B-V)$ color curve can thus be used to estimate host reddening (Folatelli et al. 2010; Burns et al. 2014). The host reddening can also be estimated from the colors at maximum light. The difference between the ob-

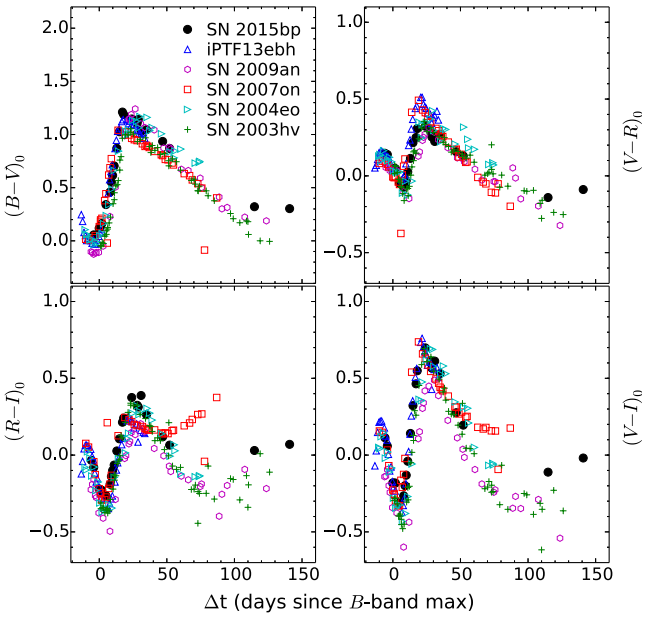

Figure 4. Reddening corrected color curves of SN 2015bp, plotted along with color curves of transitional SNe Ia iPTF13ebh (H15), 2009an (Sahu et al. 2013), 2007on (Stritzinger et al. 2011), 2004eo (Pastorello et al. 2007) and 2003hv (Leloudas et al. 2009).

served and expected colors around maximum light provides the color excess due to the host environment (Phillips et al. 1999; Altavilla et al. 2004; Folatelli et al. 2010). Wang et al. (2005) found a strong correlation between the $(B-V)$ color at 12 days past B maximum (ΔC_{12}) and $\Delta m_{15}(B)$ for SNe Ia which have suffered low reddening due to their host. Our light curves of SN 2015bp don't have a dense temporal coverage between 30 to 90 days since B-band maximum. Thus, the colors at maximum light and ΔC_{12} have been used in order to estimate host reddening.

We derive color excesses of $E(B-V)_{host} = 0.001$, -0.024 and 0.058 corresponding to the relations provided by Phillips et al. (1999), Altavilla et al. (2004) and Folatelli et al. (2010), respectively. The Folatelli et al. (2010) relation is redder than the other two relations, with a root mean square of 0.06 mag. From the ΔC_{12}-$\Delta m_{15}(B)$ correlation of Wang et al. (2005), we derive $E(B-V)_{host} = -0.05$. We therefore conclude that SN 2015bp has suffered very little (if any) reddening due to its host, which is consistent with its position in the outskirts of S0 galaxy NGC 5839, and also the fact that we see no evidence of Na I D absorption lines in the spectra. We thus use $E(B-V)_{total} = E(B-V)_{MW} = 0.046$ (Schlafly & Finkbeiner 2011) for SN 2015bp in the subsequent analysis.

4 SPECTROSCOPIC ANALYSIS

4.1 Spectral Evolution and SYN++ fits

The HCT spectra of SN 2015bp between -4.1d to $+93.9$d are presented here, along with unpublished HCT spectra of

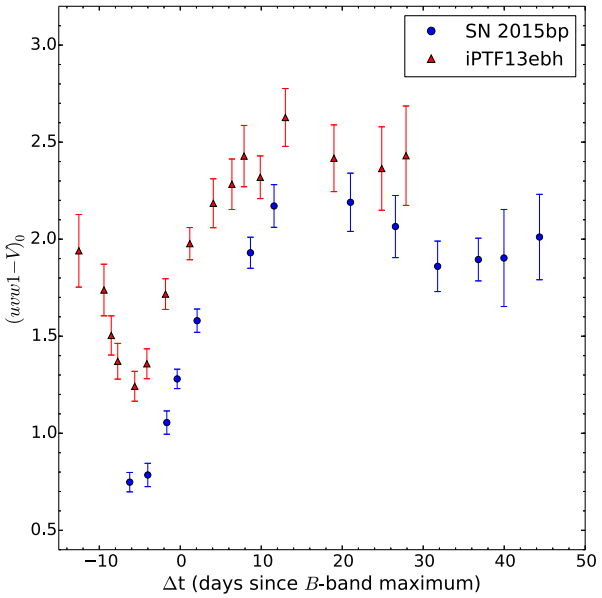

Figure 5. Reddening corrected $(uvw1-V)$ color curves of SN 2015bp and iPTF13ebh. SN 2015bp is clearly bluer than iPTF13ebh, placing it in the NUV-blue group (Milne et al. 2013).

iPTF13ebh between -10.1d to $+33.7$d. The -11.1d spectrum of iPTF13ebh was published in H15. The spectral evolution of SN 2015bp and iPTF13ebh is shown in Figure 6 and Figure 7, respectively.

The spectra of SN 2015bp and iPTF13ebh near the epoch of B-band maximum are shown in Figures 8 and 9, along with spectra of SN 2004eo (Pastorello et al. 2007), SN 2007on (Silverman et al. 2012) and SN 2011fe (Pereira et al. 2013) at similar epochs for comparison. The spectra of SN 2004eo, SN 2007on and SN 2011fe used for comparison were downloaded from the WISeREP archive[2] (Yaron & Gal-Yam 2012). The spectra were corrected for recession velocity of the respective host galaxies. The spectra of SN 2015bp and iPTF13ebh near maximum light by and large resemble those of normal SNe Ia, with a blue continuum and conspicuous Si II absorption features. Other prominent features include S II, Ca II, Fe II, Mg II and O I (see Kirshner et al. 1993). Although most of the spectral features are similar, the transitional events show a prominent absorption trough near 4200 Å attributed to Mg II and Fe III (H15), which is less pronounced in the normal SN 2011fe. Also, the O I λ7774 feature is stronger in the transitional and 1991bg-like events when compared to normal SNe Ia (Taubenberger et al. 2008).

Si II λ5972 feature is strong relative to the Si II λ6355 feature in the early spectra for both events, which is a signature of fast declining SNe Ia (eg. Hachinger et al. 2008). $\mathcal{R}$(Si II), which is a measure of the relative strengths of Si II λ5972 and λ6355 features, was first introduced by Nugent et al. (1995) as the ratio of depths of the two features. Fast declining SNe Ia ($\Delta m_{15}(B) \gtrsim 1.4$) typically show higher values of $\mathcal{R}$(Si II) ($\gtrsim 0.4$). We measure $\mathcal{R}$(Si II) of 0.55 for SN 2015bp and 0.63 for iPTF13ebh near the epoch of their respective B

[2] http://wiserep.weizmann.ac.il/

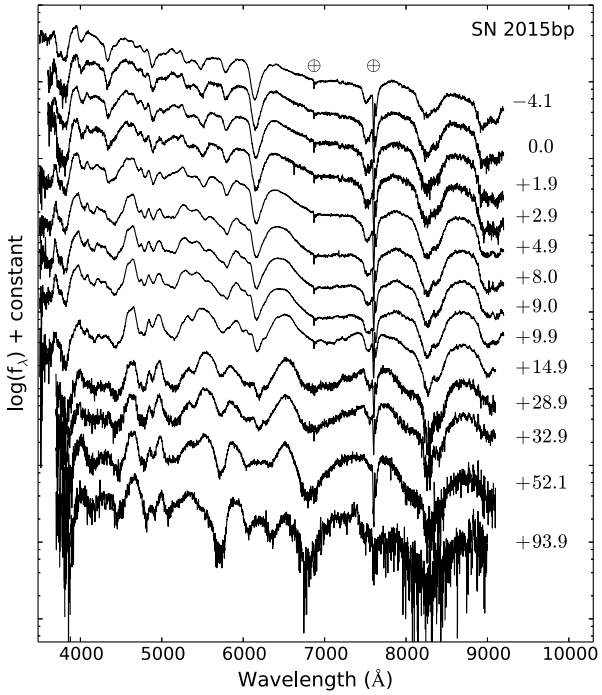

Figure 6. Spectral time series of SN 2015bp between −4.1 and +93.9 days since B-band maximum.

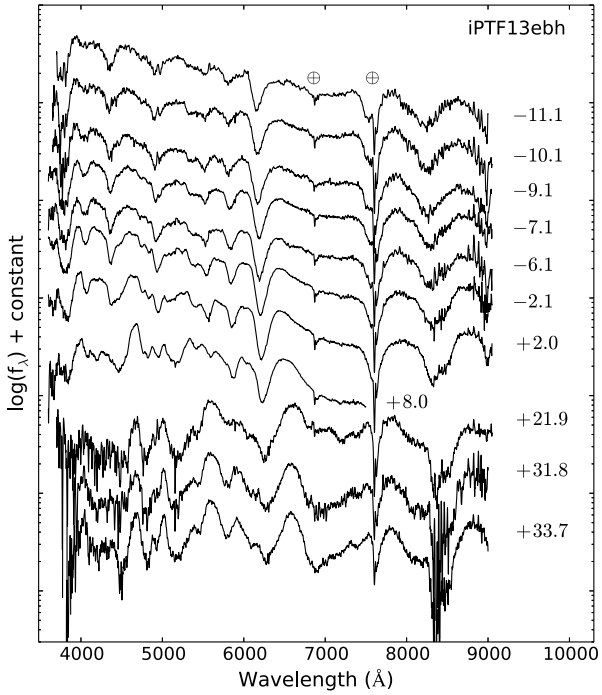

Figure 7. Spectral time series of iPTF13ebh between −11.1 and +33.7 days since B-band maximum.

maxima. The $\mathcal{R}$(Si II) measurement places iPTF13ebh close to the more extreme transitional Ia 1986G (Phillips et al. 1987) and the 1991bg-like SN 2005bl (Taubenberger et al. 2008).

Pre-maximum spectra of SNe Ia often show the presence of carbon, mostly in the form of the C II λ6580 feature (eg. Thomas et al. 2011b; Parrent et al. 2011; Folatelli et al. 2012; Silverman & Filippenko 2012), seen as a notch redward of the Si II λ6355 feature. This feature was first attributed to carbon by Branch et al. (2003). Detection of C II λ6580 in the early optical spectra of iPTF13ebh was reported by H15, who confirmed the presence of carbon by detecting strong C I features in its NIR spectra. We detect C II in our −11.1d spectrum of iPTF13ebh, beyond which it becomes difficult to discern. For SN 2015bp, we clearly detect the C II λ6580 feature in both the −4.1d and 0.0d spectra. C II features usually disappear well before B-band maximum (Thomas et al. 2011b; Parrent et al. 2011; Folatelli et al. 2012; Silverman & Filippenko 2012). There are only a few examples where C II features linger till or beyond the epoch of B maximum, most notably SN 2002fk (Cartier et al. 2014), where C II features were seen to persist ~ 8 days past the epoch of B maximum. The presence of optical C II in SN 2015bp till maximum light and presence of strong NIR C I in the spectra of iPTF13ebh (H15) provides evidence of significant unburned material in both these events.

In Figures 10-11, we show the spectra of SN 2015bp and iPTF13ebh between $\sim 7-60$ days since B maximum, compared with spectra of SN 2004eo (Pastorello et al. 2007), SN 2007on (Silverman et al. 2012), SN 2011fe (Pereira et al. 2013) and SN 2003du (Anupama et al. 2005) at similar epochs. Most spectral features are similar, with

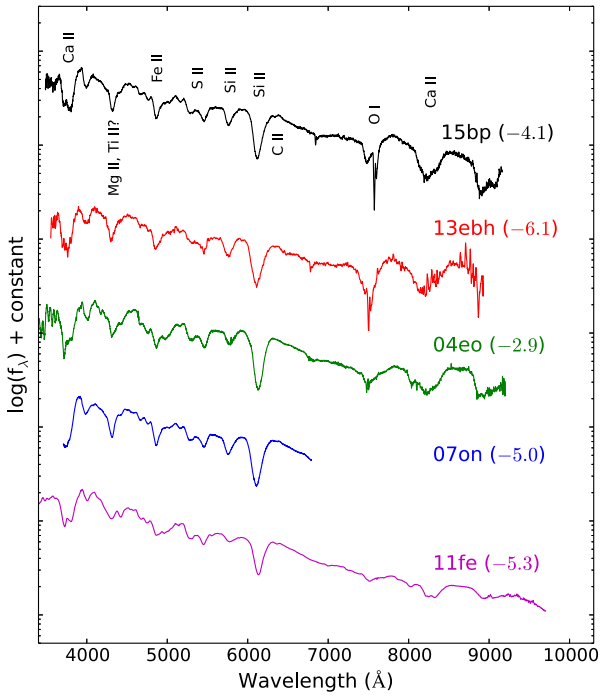

Figure 8. Pre-maximum spectra of SN 2015bp and iPTF13ebh, compared with spectra of transitional SNe Ia 2007on (Silverman et al. 2012), 2004eo (Pastorello et al. 2007) and normal Ia SN 2011fe (Pereira et al. 2013) at similar epochs.

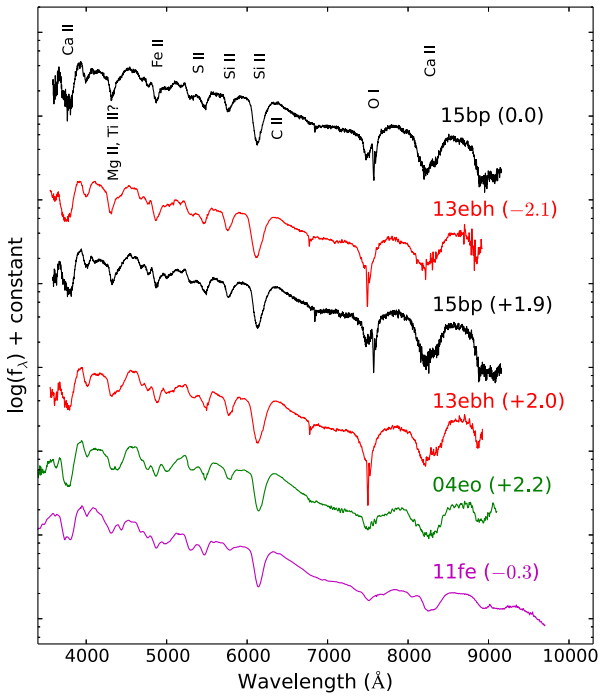

Figure 9. Spectra of SN 2015bp and iPTF13ebh near the epoch of maximum light, compared with spectra of transitional SNe Ia 2007on (Silverman et al. 2012), 2004eo (Pastorello et al. 2007) and normal Ia SN 2011fe (Pereira et al. 2013) at similar epochs.

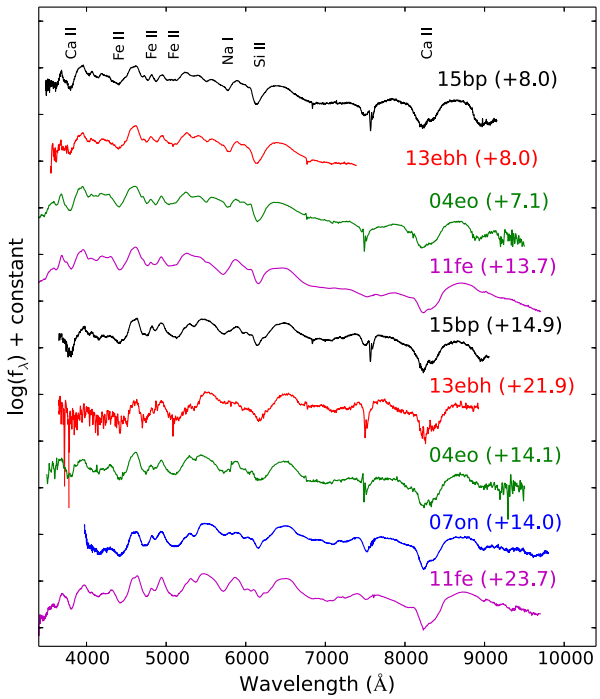

Figure 10. Comparison of spectra of SN 2015bp and iPTF13ebh between one and three weeks since B maximum with SN 2004eo (Pastorello et al. 2007), SN 2007on (Silverman et al. 2012) and SN 2011fe (Pereira et al. 2013).

the transitional events showing a higher $\mathcal{R}$(Si II) and stronger O I features. The +8.0d spectra of SN 2015bp and iPTF13ebh were seen to match well with the +13.7d spectrum of SN 2011fe. Similarly, the +14.9d spectrum of SN 2015bp showed a lot of similarity with the +21.7d and +23.7d spectra of SN 2011fe. This further highlights the rapid evolution of SN 2015bp and iPTF13ebh, which is mirrored in their color evolution (section 3.2).

Normal SNe Ia enter the nebular phase $\sim$ 100 days after B maximum when the ejecta becomes optically thin and can no longer trap γ-ray photons efficiently. Since fast decliners show a rapid evolution, they are expected to enter the nebular phase at earlier epochs. Figure 12 shows the +93.9d spectrum of SN 2015bp, plotted along with spectra of SN 2009an (Sahu et al. 2013), SN 2011fe (Pereira et al. 2013) and SN 2003du (Anupama et al. 2005) at similar epochs for comparison. Like in the SNe Ia used for comparison, the spectrum of SN 2015bp at this phase is dominated by forbidden emission lines [Fe III] λ4701, [Fe II]/[Fe III] complex $\sim$ 5300 Å and [Co III] λ5891, possibly blended with [Na I] D lines.

The width of nebular features in SNe Ia are correlated with their luminosity. Faint 1991bg-like events show the narrowest nebular features, whereas bright 1991T-like events show the broadest (eg. Mazzali et al. 1998). This can be attributed to the smaller mass of radioactive ^{56}Ni synthesized in 1991bg-like events. For the +93.9d spectrum of SN 2015bp, we measure FWHM(λ4701) $\sim 9300 \pm 100$ km s^{-1}. At a similar epoch, FWHM(λ4701) for SN 2009an is comparable ($\sim 9600 \pm 200$ km s^{-1}) to SN 2015bp, whereas that of

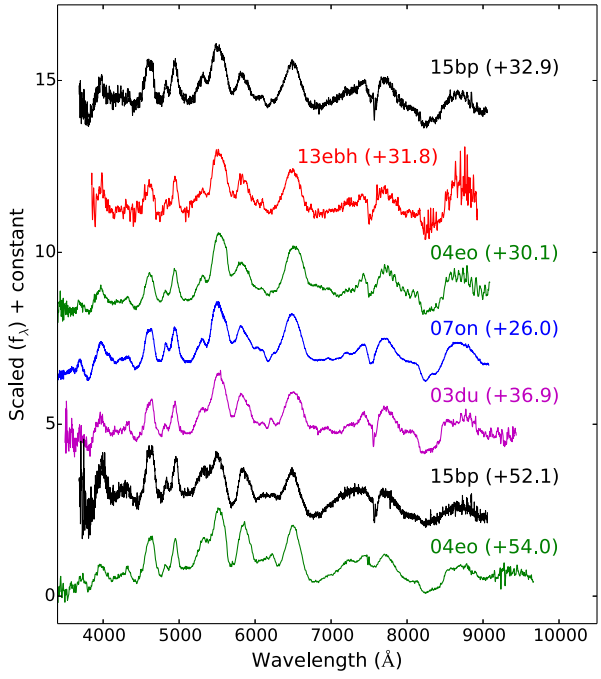

Figure 11. Comparison of spectra of SN 2015bp and iPTF13ebh between 30 and 60 days since B maximum with SN 2004eo (Pastorello et al. 2007), SN 2007on (Silverman et al. 2012), SN 2011fe (Pereira et al. 2013) and SN 2003du (Anupama et al. 2005).

the normal SNe 2011fe ($\sim 10000 \pm 100$ km s^{-1}) and 2003du ($\sim 10300 \pm 100$ km s^{-1}) is higher, as expected.

A high blueshift ($\gtrsim 1500$ km s^{-1}) in the [Fe III] λ4701 feature of SNe Ia is usually seen only in young nebular spectra obtained $< +200$ days, beyond which the central wavelength of the feature clusters around the rest wavelength (Maeda et al. 2010). The [Fe III] λ4701 blend is blueshifted by ~ 4000 km s^{-1} at +93.9d for SN 2015bp. However, velocity measurement of [Fe III] λ4701 at this early nebular epoch may be affected by P-Cygni emission from Mg II and Ti II, since the transition from the optically thick to optically thin regime may not yet be complete. The [Co III] λ5891 feature is also seen to be blueshifted but at a lower velocity of ~ 1000 km s^{-1} at +93.9d. Black et al. (2016) reported a continuous redward shift in the central wavelength of nebular features, in particular [Fe III] λ4701, starting from ~ 4600 Å at $\sim +50$ towards the rest wavelength till $\sim +300$ days in normal SNe Ia. This progressive shift, accompanied by a steady increase in line width, was attributed (in part) to emergence of weak emission on the red side of [Fe III] λ4701. Unfortunately, this trend cannot be examined further for SN 2015bp since we do not have spectra beyond +93.9d.

Additionally, the +93.9d spectrum of SN 2015bp also seems to show a narrow emission line ~ 7300 Å. This feature could be attributed to multiple species like [Fe II] $\lambda\lambda$7155, 7172, [Ca II] $\lambda\lambda$7291, 7324 or [Ni II] λ7378. However, identification of this feature with [Fe II] or [Ca II] would require it to be redshifted, whereas identification with [Ni II] would imply a blueshift of ~ 1400 km s^{-1}. Since [Fe III] and [Co III] features in the spectrum show a blueshift, we associate the feature ~ 7300 Å with [Ni II] λ7378. The [Ni II] λ7378 feature is attributed to stable ^{58}Ni which is a nuclear statistical equilibrium (NSE) product formed in the deepest layers of SN ejecta. In the DDT scenario, stable ^{58}Ni is created by the initial deflagration (Maeda et al. 2010, 2011). The [Ni II] λ7378 emission feature is usually not seen as a distinct peak till $\gtrsim 160$ days after B maximum (Silverman et al. 2013). The early emergence of this feature could be explained by a rapid decrease in opacity in outer layers of the ejecta (Krisciunas et al. 2009) and a small ejecta mass which would enable escape of γ-ray photons at earlier epochs. The small ejecta mass would also explain the fast declining light curves.

Synthetic spectra generated using SYN++ (Fisher 2000; Thomas et al. 2011a) are used to analyse the photospheric spectra of SN 2015bp near maximum light. The -4d spectrum of SN 2015bp is fit with a photospheric velocity $v_{ph} = 11000$ km s^{-1} and a blackbody temperature $T_{bb} = 10500$ K, whereas for the +4.9d spectrum we use $v_{ph} = 10000$ km s^{-1}. The absorption trough ~ 4200 Å is fit with strong Mg II, along with a small amount of Ti II. Inclusion of Ti II improves the fit marginally in the blue wing of the ~ 4200 Å absorption trough (eg. Ashall et al. 2016a). High velocity (HV) components of Ca II are generally seen in early spectra of most SNe Ia (Mazzali et al. 2005). However, like in the case of iPTF13ebh (H15), Ca II HV components are not seen in SN 2015bp. C II λ6580 is used in the -4.1 and 0.0d spectra to improve the fit redward of Si II λ6355. The C II velocity was found to be comparable to the Si II λ6355 velocity. Figure 13 shows the SYN++ fits to the early phase spectra of SN 2015bp.

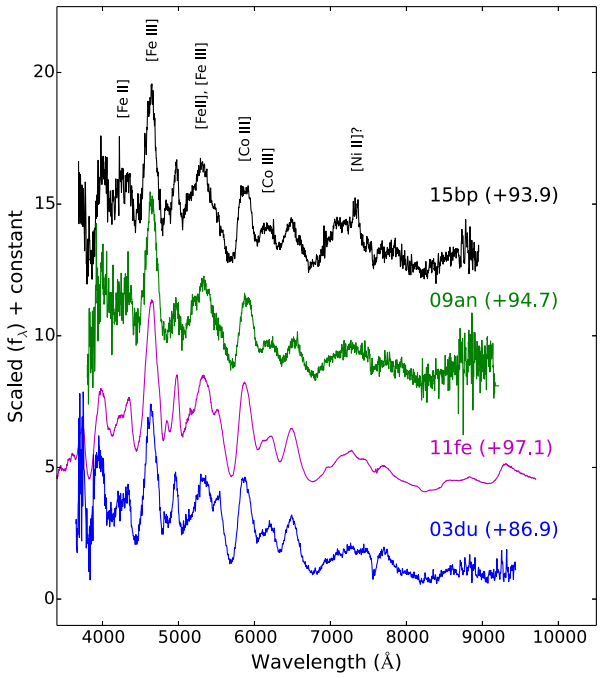

Figure 12. Comparison of +93.9d spectrum of SN 2015bp with SN 2009an (Sahu et al. 2013), SN 2011fe (Pereira et al. 2013) and SN 2003du (Anupama et al. 2005) at similar epochs.

4.2 Velocity Evolution and Spectroscopic Classification

Photospheric velocities of SN 2015bp and iPTF13ebh were measured using the absorption trough of Si II λ6355 feature. The photospheric velocity of SN 2015bp evolves from ~ 11400 km s^{-1} at -4.1d to ~ 9900 km s^{-1} at +14.9d; whereas for iPTF13ebh the photospheric velocity evolves from ~ 13600 km s^{-1} at -11.1d to ~ 8800 km s^{-1} at +21.9d. Wang et al. (2009b) classified SNe Ia into two groups - Normal (N) and High-velocity (HV) on the basis of Si II λ6355 velocity near maximum light. HV category objects were seen to cluster ~ 11800 km s^{-1}, whereas Normal category objects averaged ~ 10600 km s^{-1} (Wang et al. 2009b). With photospheric velocities of ~ 11000 km s^{-1} and ~ 10800 km s^{-1} near B maximum, SN 2015bp and iPTF13ebh are both placed in the Normal category.

Benetti et al. (2005) classified SNe Ia on the basis of the velocity gradient of Si II λ6355 feature ($\dot{v}_{Si}$). Three main subclasses of SNe Ia were found based on this definition - high velocity gradient (HVG) events ($\dot{v}_{Si} \gtrsim 70$ km s^{-1} day^{-1}), low velocity gradient (LVG) events and a third subclass of FAINT events. Objects belonging to the FAINT subclass exhibit relatively lower velocities but a rapid velocity evolution along with fast declining light curves. However, owing to the non-linear nature of the velocity evolution in most SNe Ia, the measured velocity gradient, and therefore the Benetti et al. (2005) classification could be affected by the choice of phases between which the velocity gradient is calculated. In addition, the Si II λ6355 feature weakens over time and suffers increasing contamination from other neighboring features (Blondin et al. 2012). In view of this, Blondin et al. (2012) recommended a standard definition of $\dot{v}_{Si}$ as the velocity gradient calculated between +0 and +10

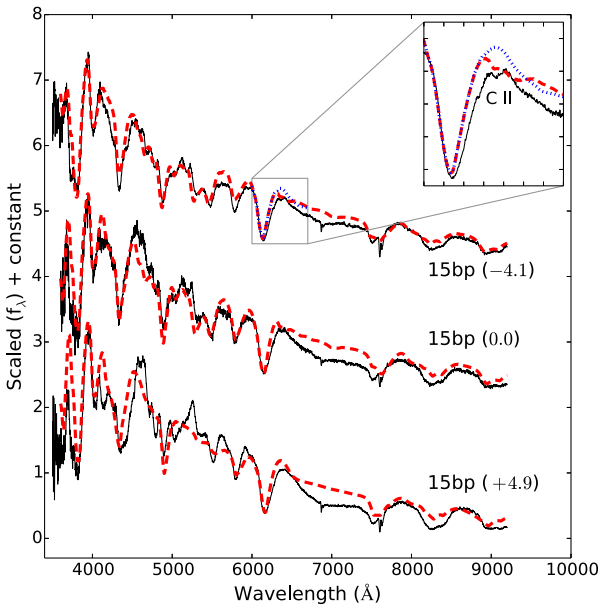

Figure 13. Spectra of SN 2015bp near maximum light plotted along with synthetic spectra generated using SYN++ (dashed lines). Inset shows how adding C II λ6580 (dashed line) improves the fit redward of Si II λ6355, as compared to when no C II is used (dotted line).

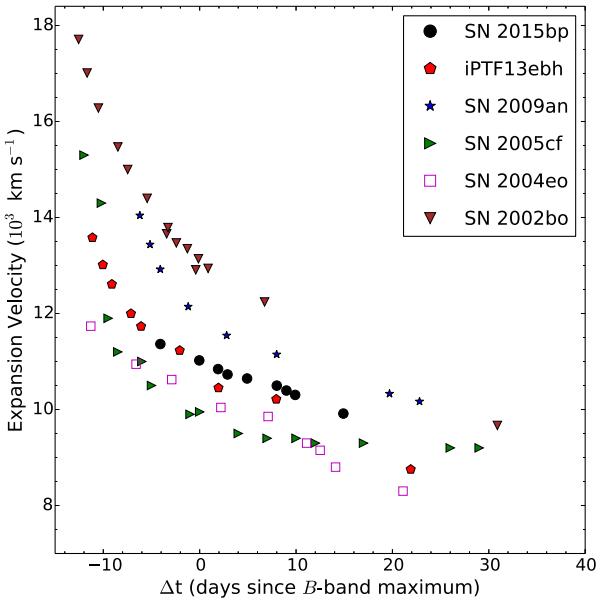

Figure 14. Velocity evolution of Si II λ6355 for SN 2015bp and iPTF13ebh, plotted along with that of SN 2009an (Sahu et al. 2013), SN 2005cf (Wang et al. 2009a), SN 2004eo (Pastorello et al. 2007) and SN 2002bo (Benetti et al. 2004).

days of B maximum.

The velocity evolution of Si II λ6355 feature for SN 2015bp and iPTF13ebh is plotted in Figure 14, along with that of SN 2009an (Sahu et al. 2013), SN 2005cf (Wang et al. 2009a), SN 2004eo (Pastorello et al. 2007) and SN 2002bo (Benetti et al. 2004). SN 2005cf is a LVG event whereas SN 2002bo is a HVG event. Among the transitional SNe in Figure 14, SN 2009an shows consistently higher velocities than the others. The velocities of SN 2015bp and iPTF13ebh are comparable during B maximum, but iPTF13ebh shows a slightly higher velocity gradient post maximum.

The velocity gradient ($\dot{v}_{Si}$) between 0 and +10 days as prescribed by Blondin et al. (2012), is 73 ± 6 km s^{-1} day^{-1} for SN 2015bp and 77 ± 5 km s^{-1} for iPTF13ebh. Benetti et al. (2005) reported $\langle \Delta m_{15}(B) \rangle = 1.83 \pm 0.09$ and $\langle \mathcal{R}(\mathrm{Si\,II}) \rangle = 0.58 \pm 0.05$ for their FAINT sample. Both SN 2015bp and iPTF13ebh lie in the FAINT subclass, but exhibit lower velocity gradients when compared to transitional events such as SN 2004eo (Pastorello et al. 2007, $\sim$ 84 km s^{-1} day^{-1}) and 2009an (Sahu et al. 2013, $\sim$ 93 km s^{-1} day^{-1}), and 1991bg-like events such as SN 2005ke (Blondin et al. 2012, $\sim$ 125 km s^{-1} day^{-1}) and SN 2005bl (Taubenberger et al. 2008, $\sim$ 120 km s^{-1} day^{-1}).

Branch et al. (2006) constructed an alternative classification scheme wherein the ratio of pEWs of Si II λ5972 and Si II λ6355 was used to divide SNe Ia into four subclasses - Core Normal (CN), Broad Line (BL), Shallow Silicon (SS) and Cool (CL). The CN subclass is tightly clustered, forming the most homogeneous subclass (Branch et al. 2006). Although the pEW(λ5972) of BL objects is comparable to CN objects, the BL subclass shows a broader λ6355 absorption feature, i.e. higher pEW(λ6355) (Branch et al. 2006). The CL subclass usually consists of low luminosity events with a conspicuous Si II λ5972 feature and an absorption trough near 4200 Å which is associated with Ti II features, indicating a cool ejecta (Branch et al. 2006; Blondin et al. 2012). By and large, the FAINT subclass of Benetti et al. (2005) corresponds to the CL subclass of Branch et al. (2006); the HVG subclass corresponds to the BL subclass and the LVG subclass includes objects belonging to both CN and SS subclasses (Branch et al. 2009).

The spectroscopic classification of SN 2015bp and iPTF13ebh according to the Branch et al. (2006) scheme is shown in Figure 15. H15 measured pEW(λ5972) and pEW(λ6355) for iPTF13ebh as 48.9 ± 0.6 and 125.2 ± 0.5, respectively. For SN 2015bp, the measured values of pEW(λ5972) and pEW(λ6355) are 37.2 ± 1 and 113.8 ± 2. Since pEW(λ5972) > 30 Å for both events, they are placed in the CL subclass (Folatelli et al. 2013). The absorption complex $\sim$ 4200 Å in maximum light spectra is attributed to Mg II and Fe III in normal SNe Ia. However, in 1991bg-like SNe Ia, this region is dominated by Ti II. The pEW of this absorption region, pEW(Mg II) or pEW3 $\gtrsim$ 220 Å for SN 1991bg-like events (Folatelli et al. 2013). For SN 2015bp, we measure a pEW3 of 74±2 Å whereas H15 measured a pEW3 of 104 ± 1 Å for iPTF13ebh. Clearly, both SN 2015bp and iPTF13ebh are spectroscopically distinct from the 1991bg class of SNe Ia.

5 DISTANCE, ABSOLUTE MAGNITUDES AND BOLOMETRIC LIGHT CURVE

SN 2015bp exploded in the outskirts of the S0 galaxy NGC 5839. The distance to NGC 5839 has been estimated using Surface Brightness Fluctuations (SBF) and Fundamental Plane (FP) methods by Tully et al. (2013), who reported a distance modulus $\mu_1 = 31.78 \pm 0.17$ mag, compatible with $H_0 = 74.4$ km s^{-1} Mpc^{-1}. Adopting $H_0 = 72$

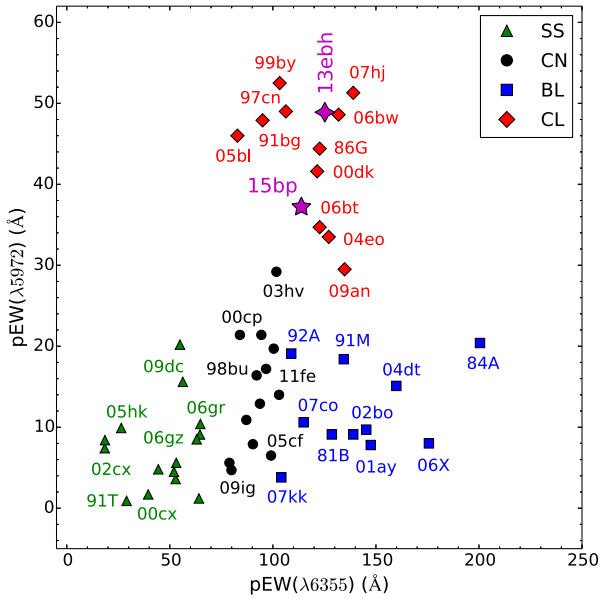

Figure 15. Spectroscopic classification of SN 2015bp and iPTF13ebh according to the Branch et al. (2006) scheme using pEW(5972) and pEW(6355). The sample of SNe Ia is taken from Branch et al. (2006) and Blondin et al. (2012), to which we added SN 2009an (Sahu et al. 2013).

km s^{-1} Mpc^{-1} (Freedman et al. 2001), the distance modulus becomes $\mu_1 = 31.85 \pm 0.17$ mag. The distance estimated using the mean Tully Fisher Relation (TFR) by Theureau et al. (2007) is higher, with $\mu_2 = 32.15 \pm 0.40$ mag. The corresponding distances are $d_1 = 23.44^{+1.91}_{-1.76}$ Mpc and $d_2 = 26.92^{+5.44}_{-4.53}$ Mpc. The absolute magnitudes and bolometric properties of SN 2015bp are computed here for the two distance scenarios d_1 (SBF/FP) and d_2 (mean TFR).

We construct the quasi-bolometric light curve of SN 2015bp using the broadband UV $uvw1, uvm2, uvw2$ and optical $UBVRI$ magnitudes presented in section 3.1. The observed magnitudes were first corrected for a total reddening of $E(B-V) = 0.046$ (section 3.3). In order to correct the UV magnitudes for reddening, we use the extinction coefficients given by Brown et al. (2010). The $UBVRI$ extinction corrected magnitudes were converted to monochromatic fluxes using the zero-points provided by Bessell et al. (1998). The UV magnitudes were converted to fluxes following Poole et al. (2008). A cubic spline function was fit through the monochromatic fluxes and integrated within appropriate wavelength limits to obtain the UV-optical quasi-bolometric flux. In order to account for missing NIR flux, we use NIR corrections prescribed by Scalzo et al. (2014a). NIR corrections were calculated for SN 2015bp by averaging the predicted NIR contribution for three events from the sample of Scalzo et al. (2014a) - SNF 20061020-000, SNF 20080918-004 and SN 2008ec, whose peak B-band luminosity was comparable to SN 2015bp. NIR corrections were taken into account between ~ -6 to $\sim +52$ days. The bolometric light curve of iPTF13ebh(1600–18000 Å) was constructed using the UV magnitudes from SOUSA archive (Brown et al. 2014) and optical-NIR magnitudes published in H15. For SN 2015bp, the peak UV contribution to the integrated (1600-23900 Å) bolometric flux is $\sim 9\%$, occurring ~ 4 days before B maximum. In contrast, the UV contribution to the bolometric flux for the normal SN 2013dy was $\sim 19\%$ (Pan et al. 2015) and $\sim 13\%$ for SN 2011fe (Pereira et al. 2013). NIR contribution to bolometric flux is not expected to be high during early epochs. For SN 2004eo, NIR contribution during maximum light was $\sim 2-3\%$, increasing to $> 20\%$ by +50d (Pastorello et al. 2007). Similarly, the NIR contribution increased from $\sim 5\%$ at +4d to $\sim 20\%$ at +30 for the normal SN 2005cf (Wang et al. 2009a). Contribution of the NIR correction applied to SN 2015bp increases from $\sim 12\%$ near maximum to $\sim 23\%$ at +30d. The extinction corrected peak apparent and absolute magnitudes of SN 2015bp for the two distance scenarios are tabulated in Table 6.

Normal SNe Ia ($\Delta m_{15} \lesssim 1.7$) generally follow the width-luminosity relation or Phillip's relation (Phillips 1993), i.e. the absolute magnitudes are correlated with the decline rate parameter Δm_{15} (eg. Hamuy et al. 1996; Phillips et al. 1999; Altavilla et al. 2004; Reindl et al. 2005; Prieto et al. 2006). However, the Phillip's relation shows a sudden steepening for events with $\Delta m_{15} \gtrsim 1.7$, which cannot be accounted for by extending the linear or quadratic Phillip's relation. Garnavich et al. (2004) and Taubenberger et al. (2008) provided correlations between absolute magnitude and decline rate for fast decliners with $\Delta m_{15} \gtrsim 1.7$. Using these steeper relations, we derive M_B^{max} of -18.30 ± 0.20 and -18.40 ± 0.20 for SN 2015bp, respectively. Wang et al. (2005) found a linear correlation between ΔC_{12} and M_λ^{max} for events with $0.81 \lesssim \Delta m_{15}(B) \lesssim 1.95$, which spans a wide range of peak luminosity. For a ΔC_{12} of 0.79 for SN 2015bp, the relation yields $M_B^{max} = -18.43 \pm 0.18$. The absolute magnitudes of SN 2015bp under the d_2 scenario are compatible with these estimates (Table 6).

Ashall et al. (2016b) studied the luminosity distribution of SNe Ia in different host environments. For a sample of 16 SNe Ia in passive (E and S0) galaxies, the extinction corrected mean peak B and V-band absolute magnitudes were reported as $\overline{M_B^{max}} = -18.57 \pm 0.24$ and $\overline{M_V^{max}} = -18.71 \pm 0.18$. The peak absolute magnitudes of SN 2015bp (for both distance scenarios) are fainter than the mean values of Ashall et al. (2016b), which is expected since the mean decline rate for their passive galaxy sample, $\overline{\Delta m_{15}(B)} \sim 1.4$, which is lower than that of SN 2015bp.

It is interesting to note here that in spite of the overall photometric and spectroscopic similarities between SN 2015bp and iPTF13ebh, H15 reported $M_B^{max} = -18.95 \pm 0.19$ and $M_V^{max} = -19.01 \pm 0.18$ for iPTF13ebh, significantly more luminous than SN 2015bp. iPTF13ebh falls within the Phillip's relation and becomes "overluminous" when compared to the steeper relations of Garnavich et al. (2004), Taubenberger et al. (2008) and Wang et al. (2005). SN 2007on (Stritzinger et al. 2011), which has a similar color-stretch parameter $s_{BV} = 0.55 \pm 0.02$ (H15), also has a luminosity comparable to SN 2015bp (d_2 scenario) with $M_B^{max} = -18.54 \pm 0.15$ and $M_V^{max} = -18.67 \pm 0.15$.

The bolometric light curves of SNe Ia are powered by the decay chain ^{56}Ni $\rightarrow$ ^{56}Co $\rightarrow$ ^{56}Fe. Bolometric light curve shape depends on total ejected mass, ejected ^{56}Ni mass, explosion energy and opacity (Arnett 1982; Mazzali et al. 2007). In order to estimate the physical parameters of SN 2015bp like ^{56}Ni mass ($M_{\rm Ni}$), total ejected mass ($M_{\rm ej}$) and kinetic energy of the explosion ($E_{\rm k}$), we use the Arnett–Valenti model presented by Valenti et al. (2008).

Table 6. Reddening corrected peak magnitudes of SN 2015bp and predicted absolute magnitudes based on different calibrations of the width-luminosity relation, all of which are scaled to $H_0 = 72$ km s^{-1} Mpc^{-1}.

Filter	T^*_{max} (days)	Decline Rate Δm_{15}	Peak apparent magnitude	Peak absolute magnitude $\mu_1 = 31.85$	$\mu_2 = 32.15$
$uvw2$	−3.0	1.67 ± 0.13	15.88 ± 0.07	−15.97 ± 0.19	−16.27 ± 0.41
$uvm2$	−3.4	1.88 ± 0.15	16.15 ± 0.08	−15.70 ± 0.19	−16.00 ± 0.41
$uvw1$	−4.1	1.67 ± 0.10	14.65 ± 0.05	−17.20 ± 0.18	−17.50 ± 0.40
U	−1.3	1.95 ± 0.08	13.35 ± 0.05	−18.50 ± 0.17	−18.80 ± 0.40
B	0.0	1.72 ± 0.04	13.79 ± 0.03	−18.06 ± 0.17	−18.36 ± 0.40
V	−0.2	0.79 ± 0.04	13.67 ± 0.03	−18.18 ± 0.17	−18.48 ± 0.40
R	+1.0	0.67 ± 0.03	13.63 ± 0.02	−18.22 ± 0.17	−18.52 ± 0.40
I	−4.1	0.43 ± 0.04	13.81 ± 0.03	−18.04 ± 0.17	−18.34 ± 0.40

Relation	M_B^{max}	M_V^{max}	M_R^{max}	M_I^{max}
Prieto et al. (2006)	−18.93 ± 0.19	−18.87 ± 0.16	−18.90 ± 0.17	−18.66 ± 0.18
Garnavich et al. (2004)	−18.30 ± 0.20	−18.61 ± 0.20		−18.38 ± 0.20
Taubenberger et al. (2008)	−18.40 ± 0.20	−18.52 ± 0.20		
Wang et al. (2005)	−18.43 ± 0.18	−18.57 ± 0.16		−18.42 ± 0.16

*time since B-band max (JD 2457113.33)

The model assumes spherical symmetry, homologous expansion of ejecta, no mixing of ^{56}Ni, a small pre-explosion radius and a constant opacity ($\kappa_{\rm opt}$). The ejecta is assumed to be in the photospheric phase, which means that the Arnett–Valenti relation is valid only for $\lesssim 30$ days past explosion. The free parameters in the model are $M_{\rm Ni}$ and $\tau_{\rm m}$, where the latter is the time-scale of the light curve, defined as

$$\tau_{\rm m} = \left(\frac{\kappa_{\rm opt}}{\beta c}\right)^{1/2} \left(\frac{6M_{\rm ej}^3}{5E_{\rm k}}\right)^{1/4} \quad (1)$$

Here, $\beta \approx 13.8$ is a constant of integration (Arnett 1982) and we use a constant $\kappa_{\rm opt} = 0.07$ cm^2 g^{-1} (eg. Toy et al. 2016). For a uniform density (Arnett 1982), the kinetic energy can be expressed as

$$E_{\rm k} \approx \frac{3}{5}\frac{M_{\rm ej} v_{\rm ph}^2}{2} \quad (2)$$

The photospheric velocity $v_{\rm ph}$ can be constrained using the spectra. Once $\tau_{\rm m}$ is obtained by fitting the bolometric light curve to the model, Equations (1) and (2) can be used to derive $M_{\rm ej}$ and $E_{\rm k}$.

Fitting the model to the early part of the bolometric light curve of SN 2015bp, we obtain best-fitting parameter values of $\tau_{\rm m} = 8.79 \pm 0.54$ days, $M_{\rm Ni} = 0.15 \pm 0.01$ and 0.20 ± 0.01 M$_\odot$, for d_1 and d_2, respectively. Fixing $v_{\rm ph} = 11000 \pm 500$ km s^{-1} as the Si II velocity near maximum, we derive $M_{\rm ej} = 0.94^{+0.17}_{-0.15}$ M$_\odot$ and $E_{51} = 0.68^{+0.19}_{-0.16}$ erg. For iPTF13ebh, the best-fitting parameters obtained are $\tau_{\rm m} = 10.26 \pm 1.05$ days and $M_{\rm Ni} = 0.28 \pm 0.03$ M$_\odot$. Fixing $v_{\rm ph} = 10800 \pm 500$ km s^{-1} for iPTF13ebh, we derive $M_{\rm ej} = 1.26^{+0.34}_{-0.29}$ M$_\odot$ and $E_{51} = 0.88^{+0.34}_{-0.27}$ erg. The bolometric light curves of SN 2015bp and iPTF13ebh are shown in Figure 16, along with the best-fitting Arnett–Valenti models.

The model favors a low B-band rise time of ~ 14 days for both SN 2015bp and iPTF13ebh. Although normal SNe Ia have rise times of ~ 18 days (Ganeshalingam et al. 2011), faster declining SNe Ia are expected to have lower rise times. According to Scalzo et al. (2014a), the correlation between B-band rise time and decline rate is given as

$$t_{\rm R}({\rm B}) = 17.5 - 5\,(\Delta m_{15}({\rm B}) - 1.1)$$

The above relation yields rise times of 14.4 and 14.1 days for SN 2015bp and iPTF13ebh, compatible with the Arnett–Valenti model.

6 DISCUSSION AND CONCLUSIONS

We have presented HCT photometric and spectroscopic observations of transitional Ia SN 2015bp, along with unpublished HCT spectra of transitional Ia iPTF13ebh. The photometric and spectroscopic properties of SN 2015bp are intermediate to normal-bright and 1991bg-like events.

Although $\Delta m_{15}(B) = 1.72$, the I-band light curve shows a clear secondary maximum and peaks ~ 4 days prior to B maximum. SN 2015bp is therefore placed in the transitional category along with iPTF13ebh and a few other notable events (see H15, table 8).

As expected from the narrow light curves, SN 2015bp also shows a rapid color evolution. The $(B-V)$ color near maximum light is 0.12 ± 0.02 for SN 2015bp, which is slightly redder compared to normal SNe Ia but consistent with the mean value of $\overline{(B-V)} = 0.095 \pm 0.060$ for SNe Ia hosted by passive galaxies (Ashall et al. 2016b). The $(B-V)$ color curve peaks only ~ 17 days after B maximum ($s_{BV} = 0.57 \pm 0.03$). Although iPTF13ebh with $\Delta m_{15}(B) = 1.79 \pm 0.01$, $s_{BV} = 0.63 \pm 0.02$ and SN 2007on with $\Delta m_{15}(B) = 1.89 \pm 0.01$, $s_{BV} = 0.55 \pm 0.02$ (H15) are both faster declining than SN 2015bp, the inverse sequence is not seen in the color-stretch parameter s_{BV}. iPTF13ebh actually shows a higher value of s_{BV} than SN 2015bp, whereas that of SN 2007on is comparable to SN 2015bp. iPTF13ebh, with the highest s_{BV} among the three, is also the most luminous, whereas SN 2007on, with s_{BV} comparable to SN 2015bp, also has a comparable luminosity within the uncertainties (section 5). This is further evidence that s_{BV} is better suited to study fast declining events (Burns et al. 2014).

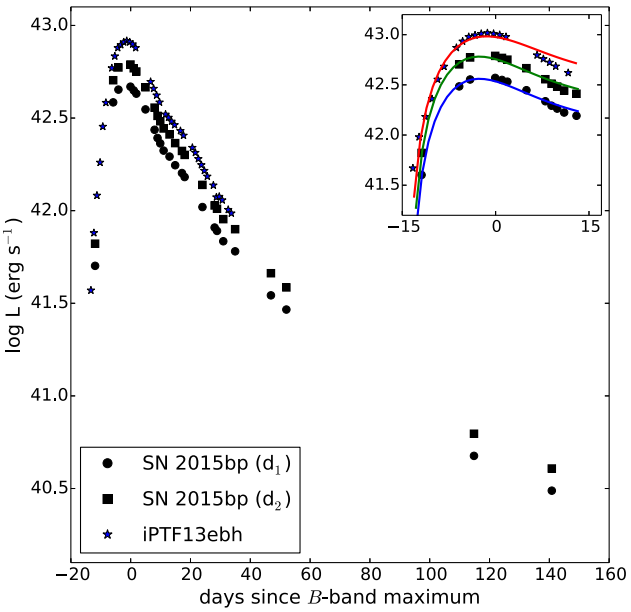

Figure 16. Bolometric light curve of SN 2015bp(1600–23900 Å) for two distance scenarios as described in the text, plotted along with the bolometric light curve of iPTF13ebh(1600–18000 Å). Inset shows early part of the bolometric light curves of SN 2015bp and iPTF13ebh along with the best-fitting Arnett–Valenti model for a rise time of ∼ 14 days for both events. The bolometric light curve and model for iPTF13ebh was shifted upwards by 0.1 dex in the inset, whereas that of SN 2015bp (d$_1$) was shifted downwards by 0.1 dex in the inset for clarity.

The $(uvw1 - V)$ color of SN 2015bp places it in the NUV-blue category (Milne et al. 2010). Although fast declining events were excluded from the analysis, Milne et al. (2013) found a low velocity gradient for each NUV-blue event in their UVOT sample. Clearly, SN 2015bp does not conform to this trend. iPTF13ebh, which was placed in the NUV-red category by H15, is also an outlier in that it shows strong carbon features, which were detected in only one NUV-red event in the sample of Milne et al. (2013). This suggests that more transitional events need to be studied in the UV in order to better understand the diversity within this subclass.

Spectra of SN 2015bp also show a rapid evolution, with $\mathcal{R}$(Si II) = 0.55, whereas $\mathcal{R}$(Si II) = 0.63 for iPTF13ebh near maximum light. The presence of C II λ6580 till the epoch of maximum light indicates a significant amount of unburned material in SN 2015bp. The +93.9d spectrum of SN 2015bp shows an unusual emission feature ∼ 7300 Å, which we associate with Ni II λ7378 (Section 4.1). The early appearance of this narrow feature points toward a small ejecta mass, which is consistent with our estimates of M_{ej} from the bolometric light curve. The velocity gradient of Si II λ6355 and the pEW measurements of Si II $\lambda\lambda$6355, 5972 place SN 2015bp and iPTF13ebh in the CL and FAINT subclasses of Branch et al. (2006) and Benetti et al. (2005) alongside other transitional events (Section 4.2). Although iPTF13ebh is more luminous, the $\mathcal{R}$(Si II) and pEW measurements indicate that iPTF13ebh is spectroscopically more 'extreme' than SN 2015bp. H15 noted that many of the NIR spectroscopic properties of iPTF13ebh are similar to the 1991bg-like SN 1999by. This further highlights the diversity within the subclass of transitional SNe Ia and emphasizes the need to study more such events in detail.

In the d$_2$ (mean TFR) distance scenario, the absolute magnitudes $M_B^{max} = -18.36 \pm 0.40$ and $M_V^{max} = -18.48 \pm 0.40$ for SN 2015bp, which are consistent with the estimates from the steeper width-luminosity relations of Garnavich et al. (2004) and Taubenberger et al. (2008), and the ΔC_{12}-luminosity relation of Wang et al. (2005). Also, the d$_2$ luminosity of SN 2015bp is closer to the mean observed luminosity of SNe Ia hosted by passive galaxies (Ashall et al. 2016b). Fitting the bolometric (1600–23900 Å) light curve of SN 2015bp with the Arnett–Valenti model indicates a ^{56}Ni mass $M_{\rm Ni} \sim 0.2$ M$_\odot$, total ejected mass $M_{\rm ej} \sim 0.9$ M$_\odot$ and kinetic energy $E_{51} \sim 0.7$ erg. The mass of ^{56}Ni synthesized in SN 2015bp is much lower than the typical value for normal SNe Ia (∼ 0.6 M$_\odot$) but slightly higher than what is seen for subluminous 1991bg-like events (∼ 0.1 M$_\odot$).

Chandrasekhar mass DDT models are capable of producing a large range of ^{56}Ni mass of $\sim 0.2 - 1.1$ M$_\odot$ (eg. Kasen et al. 2009; Seitenzahl et al. 2013; Sim et al. 2013), accounting for most SNe Ia observed in nature. Double detonation models of sub-Chandrasekhar WDs can produce a similar range of ^{56}Ni mass (eg. Fink et al. 2010; Sim et al. 2010). Recently, the violent merger scenario involving a double degenerate system (Pakmor et al. 2010, 2011) has garnered a lot of attention. Violent mergers have been considered as plausible progenitor scenarios for peculiar SN 2002es-like events which include PTF10ops (Maguire et al. 2011), SN 2010lp (Kromer et al. 2013b) and iPTF14atg (Kromer et al. 2016). The brightness distribution of SNe Ia produced by violent merger models is compatible with observations (Ruiter et al. 2013). Pure deflagrations of Chandrasekhar mass WDs leaving a bound remnant (eg. Jordan et al. 2012; Kromer et al. 2013a) produce weak explosions at the lower end of the $M_{\rm ej} - M_{\rm Ni}$ distribution for SNe Ia, whose overall properties resemble those of peculiar SN 2002cx-like events rather than normal SNe Ia.

The $M_{\rm ej}$ and $M_{\rm Ni}$ estimates obtained for SN 2015bp in section 5 disfavour a Chandrasekhar mass progenitor scenario. Furthermore, three-dimensional simulations of DDT models (Seitenzahl et al. 2013) predict stable iron-group isotopes at intermediate velocities (∼3000 to 10000 km s^{-1}), in conflict with low velocity [Ni II] detected for SN 2015bp. For their $m_{\rm WD} = 0.97$ M$_\odot$ double detonation model, Sim et al. (2010) derived $M_{\rm Ni} = 0.30$ M$_\odot$, $\Delta m_{15}(B) = 1.73$ and $M_{\rm B}^{\rm max} = -18.5$. The decline rate and B-band luminosity observed for SN 2015bp is consistent with this model. Although the model predicts a higher ^{56}Ni yield, the predicted rise time of ∼ 20 days is also significantly higher than what was inferred for SN 2015bp (∼ 14 days). The lower inferred rise time for SN 2015bp could be attributed to presence of ^{56}Ni in the outer layers of the ejecta (see Hoeflich & Khokhlov 1996).

An alternative for SN 2015bp could be the violent merger scenario, wherein the SN luminosity depends on the mass of the sub-Chandrasekhar primary CO WD undergoing prompt detonation during the merger. For a primary

WD mass of $m_{\rm WD} = 0.97$ M$_\odot$, Ruiter et al. (2013) derived a peak bolometric magnitude of $M_{\rm bol} = -18.20$. The observed peak bolometric magnitude for SN 2015bp (-18.0 to -18.3) is consistent with this model. Favouring a specific sub-Chandrasekhar scenario for SN 2015bp would require detailed hydrodynamic simulations.

For iPTF13ebh, our estimates of the explosion parameters do not rule out a Chandrasekhar mass progenitor scenario. H15 invoked a DDT model corresponding to a ^{56}Ni mass of 0.27 M$_\odot$ provided by Höflich et al. (2002) to explain the observed properties of iPTF13ebh. Our estimates of $M_{\rm Ni} \sim 0.3$ M$_\odot$ and $M_{\rm ej} \sim 1.3$ M$_\odot$ are compatible with their model.

ACKNOWLEDGEMENTS

We thank the staff of IAO, Hanle and CREST, Hosakote, that made these observations possible. The facilities at IAO and CREST are operated by the Indian Institute of Astrophysics, Bangalore. We also thank all HCT observers who spared part of their observing time for supernova observations. This work has made use of the NASA Astrophysics Data System and the NED which is operated by Jet Propulsion Laboratory, California Institute of Technology, under contract with the National Aeronautics and Space Administration. This work made use of Swift/UVOT data reduced by P. J. Brown and released in the Swift Optical/Ultraviolet Supernova Archive (SOUSA). SOUSA is supported by NASA's Astrophysics Data Analysis Program through grant NNX13AF35G. This work also made use of the Weizmann interactive supernova data repository (WISeREP). We thank Stephane Blondin for sharing velocity gradient data and Richard Scalzo for sharing NIR correction data. We would also like to thank the anonymous referee whose insightful comments helped improve the quality of this manuscript.

REFERENCES

Altavilla G., et al., 2004, MNRAS, 349, 1344
Anupama G. C., Sahu D. K., Jose J., 2005, A&A, 429, 667
Arnett W. D., 1982, ApJ, 253, 785
Ashall C., Mazzali P. A., Pian E., James P. A., 2016a, MNRAS,
Ashall C., Mazzali P., Sasdelli M., Prentice S. J., 2016b, MNRAS, 460, 3529
Benetti S., et al., 2004, MNRAS, 348, 261
Benetti S., et al., 2005, ApJ, 623, 1011
Bessell M. S., Castelli F., Plez B., 1998, A&A, 333, 231
Black C. S., Fesen R. A., Parrent J. T., 2016, MNRAS, 462, 649
Blondin S., et al., 2012, AJ, 143, 126
Branch D., et al., 2003, AJ, 126, 1489
Branch D., et al., 2006, PASP, 118, 560
Branch D., Chau Dang L., Baron E., 2009, PASP, 121, 238
Breeveld A. A., Landsman W., Holland S. T., Roming P., Kuin N. P. M., Page M. J., 2011, in McEnery J. E., Racusin J. L., Gehrels N., eds, AIP Conf. Series Vol. 1358, Am. Inst. Phys., New York. pp 373–376 (arXiv:1102.4717), doi:10.1063/1.3621807
Brown P. J., et al., 2009, AJ, 137, 4517
Brown P. J., et al., 2010, ApJ, 721, 1608
Brown P. J., Breeveld A. A., Holland S., Kuin P., Pritchard T., 2014, Ap&SS, 354, 89
Burns C. R., et al., 2011, AJ, 141, 19
Burns C. R., et al., 2014, ApJ, 789, 32
Cardelli J. A., Clayton G. C., Mathis J. S., 1989, ApJ, 345, 245
Cartier R., et al., 2014, ApJ, 789, 89
Filippenko A. V., 1997, ARA&A, 35, 309
Fink M., Röpke F. K., Hillebrandt W., Seitenzahl I. R., Sim S. A., Kromer M., 2010, A&A, 514, A53
Fisher A. K., 2000, PhD thesis, The University of Oklahoma
Folatelli G., et al., 2010, AJ, 139, 120
Folatelli G., et al., 2012, ApJ, 745, 74
Folatelli G., et al., 2013, ApJ, 773, 53
Foley R. J., et al., 2012, ApJ, 753, L5
Freedman W. L., et al., 2001, ApJ, 553, 47
Ganeshalingam M., Li W., Filippenko A. V., 2011, MNRAS, 416, 2607
Garnavich P. M., et al., 2004, ApJ, 613, 1120
Gehrels N., et al., 2004, ApJ, 611, 1005
Hachinger S., Mazzali P. A., Tanaka M., Hillebrandt W., Benetti S., 2008, MNRAS, 389, 1087
Hamuy M., Phillips M. M., Suntzeff N. B., Schommer R. A., Maza J., Aviles R., 1996, AJ, 112, 2391
Hillebrandt W., Niemeyer J. C., 2000, ARA&A, 38, 191
Hillebrandt W., Kromer M., Röpke F. K., Ruiter A. J., 2013, Frontiers of Physics, 8, 116
Hoeflich P., Khokhlov A., 1996, ApJ, 457, 500
Höflich P., Gerardy C. L., Fesen R. A., Sakai S., 2002, ApJ, 568, 791
Howell D. A., 2011, Nature Communications, 2, 350
Hoyle F., Fowler W. A., 1960, ApJ, 132, 565
Hsiao E. Y., et al., 2015, A&A, 578, A9
Jha S. W., Patel B., Foley R. J., 2015, The Astronomer's Telegram, 7251
Jordan IV G. C., Perets H. B., Fisher R. T., van Rossum D. R., 2012, ApJ, 761, L23
Kasen D., 2006, ApJ, 649, 939
Kasen D., Woosley S. E., 2007, ApJ, 656, 661
Kasen D., Röpke F. K., Woosley S. E., 2009, Nature, 460, 869
Khokhlov A. M., 1991, A&A, 245, 114
Kirshner R. P., et al., 1993, ApJ, 415, 589
Krisciunas K., et al., 2001, AJ, 122, 1616
Krisciunas K., et al., 2009, AJ, 138, 1584
Kromer M., et al., 2013a, MNRAS, 429, 2287
Kromer M., et al., 2013b, ApJ, 778, L18
Kromer M., et al., 2016, MNRAS, 459, 4428
Landolt A. U., 1992, AJ, 104, 340
Leibundgut B., et al., 1993, AJ, 105, 301
Leloudas G., et al., 2009, A&A, 505, 265
Li W., et al., 2011, MNRAS, 412, 1441
Lira P., 1995, Master's thesis, Univ. Chile
Livne E., Arnett D., 1995, ApJ, 452, 62
Maeda K., Taubenberger S., Sollerman J., Mazzali P. A., Leloudas G., Nomoto K., Motohara K., 2010, ApJ, 708, 1703
Maeda K., et al., 2011, MNRAS, 413, 3075
Maguire K., et al., 2011, MNRAS, 418, 747
Maoz D., Mannucci F., Nelemans G., 2014, ARA&A, 52, 107
Mazzali P. A., Cappellaro E., Danziger I. J., Turatto M., Benetti S., 1998, ApJ, 499, L49
Mazzali P. A., et al., 2005, ApJ, 623, L37
Mazzali P. A., Röpke F. K., Benetti S., Hillebrandt W., 2007, Science, 315, 825
Milne P. A., et al., 2010, ApJ, 721, 1627
Milne P. A., Brown P. J., Roming P. W. A., Bufano F., Gehrels N., 2013, ApJ, 779, 23
Modjaz M., Li W., Filippenko A. V., King J. Y., Leonard D. C., Matheson T., Treffers R. R., Riess A. G., 2001, PASP, 113, 308
Nomoto K., Thielemann F.-K., Yokoi K., 1984, ApJ, 286, 644

Nugent P., Phillips M., Baron E., Branch D., Hauschildt P., 1995, ApJ, 455, L147
Oke J. B., 1990, AJ, 99, 1621
Pakmor R., Kromer M., Röpke F. K., Sim S. A., Ruiter A. J., Hillebrandt W., 2010, Nature, 463, 61
Pakmor R., Hachinger S., Röpke F. K., Hillebrandt W., 2011, A&A, 528, A117
Pan Y.-C., et al., 2015, MNRAS, 452, 4307
Parrent J. T., et al., 2011, ApJ, 732, 30
Pastorello A., et al., 2007, MNRAS, 377, 1531
Pereira R., et al., 2013, A&A, 554, A27
Perlmutter S., et al., 1999, ApJ, 517, 565
Phillips M. M., 1993, ApJ, 413, L105
Phillips M. M., 2012, Publ. Astron. Soc. Australia, 29, 434
Phillips M. M., et al., 1987, PASP, 99, 592
Phillips M. M., Lira P., Suntzeff N. B., Schommer R. A., Hamuy M., Maza J., 1999, AJ, 118, 1766
Poole T. S., et al., 2008, MNRAS, 383, 627
Prieto J. L., Rest A., Suntzeff N. B., 2006, ApJ, 647, 501
Reindl B., Tammann G. A., Sandage A., Saha A., 2005, ApJ, 624, 532
Riess A. G., et al., 1998, AJ, 116, 1009
Roming P. W. A., et al., 2005, Space Sci. Rev., 120, 95
Ruiter A. J., et al., 2013, MNRAS, 429, 1425
Sahu D. K., Anupama G. C., Anto P., 2013, MNRAS, 430, 869
Scalzo R., et al., 2014a, MNRAS, 440, 1498
Scalzo R. A., Ruiter A. J., Sim S. A., 2014b, MNRAS, 445, 2535
Schlafly E. F., Finkbeiner D. P., 2011, ApJ, 737, 103
Schlegel D. J., Finkbeiner D. P., Davis M., 1998, ApJ, 500, 525
Seitenzahl I. R., et al., 2013, MNRAS, 429, 1156
Silverman J. M., Filippenko A. V., 2012, MNRAS, 425, 1917
Silverman J. M., et al., 2012, MNRAS, 425, 1789
Silverman J. M., Ganeshalingam M., Filippenko A. V., 2013, MNRAS, 430, 1030
Sim S. A., Röpke F. K., Hillebrandt W., Kromer M., Pakmor R., Fink M., Ruiter A. J., Seitenzahl I. R., 2010, ApJ, 714, L52
Sim S. A., et al., 2013, MNRAS, 436, 333
Stalin C. S., Hegde M., Sahu D. K., Parihar P. S., Anupama G. C., Bhatt B. C., Prabhu T. P., 2008, Bulletin of the Astronomical Society of India, 36, 111
Stritzinger M. D., et al., 2011, AJ, 142, 156
Taubenberger S., et al., 2008, MNRAS, 385, 75
Theureau G., Hanski M. O., Coudreau N., Hallet N., Martin J.-M., 2007, A&A, 465, 71
Thomas R. C., Nugent P. E., Meza J. C., 2011a, PASP, 123, 237
Thomas R. C., et al., 2011b, ApJ, 743, 27
Toy V. L., et al., 2016, ApJ, 818, 79
Tully R. B., et al., 2013, AJ, 146, 86
Valenti S., et al., 2008, MNRAS, 383, 1485
Wang X., Wang L., Zhou X., Lou Y.-Q., Li Z., 2005, ApJ, 620, L87
Wang X., et al., 2009a, ApJ, 697, 380
Wang X., et al., 2009b, ApJ, 699, L139
Woosley S. E., Weaver T. A., 1994, ApJ, 423, 371
Yamanaka M., et al., 2014, ApJ, 782, L35
Yaron O., Gal-Yam A., 2012, PASP, 124, 668